

FedMed-ATL: Misaligned Unpaired Brain Image Synthesis via Affine Transform Loss

Guoyang Xie^{*1,2} Jinbao Wang^{*1,2} Yawen Huang^{*3} Yefeng Zheng³ Feng Zheng² Yaochu Jin^{1,4}

Abstract

The existence of completely aligned and paired multi-modal neuroimaging data has proved its effectiveness in the diagnosis of brain diseases. However, collecting the full set of well-aligned and paired data is impractical or even luxurious, since the practical difficulties may include high cost, long time acquisition, image corruption, and privacy issues. Previously, the misaligned unpaired neuroimaging data (termed as MUD) are generally treated as noisy label. However, such a noisy label-based method could not work very well when misaligned data occurs distortions severely, for example, different angles of rotation. In this paper, we propose a novel federated self-supervised learning (FedMed) for brain image synthesis. An affine transform loss (ATL) was formulated to make use of severely distorted images without violating privacy legislation for the hospital. We then introduce a new data augmentation procedure for self-supervised training and fed it into three auxiliary heads, namely auxiliary rotation, auxiliary translation, and auxiliary scaling heads. The proposed method demonstrates advanced performance in both the quality of synthesized results under a severely misaligned and unpaired data setting, and better stability than other GAN-based algorithms. The proposed method also reduces the demand for deformable registration while encouraging to realize the usage of those misaligned and unpaired data. Experimental results verify the outstanding ability of our learning paradigm compared to other state-of-the-art approaches. Our code is available on the website: <https://github.com/FedMed-Meta/FedMed-ATL>.

^{*}Equal contribution ¹NICE Group, University of Surrey, Guildford, United Kingdom ²VIP Lab, Southern University of Science and Technology, Shenzhen, China ³Jarvis Lab, Tencent, Shenzhen, China ⁴Bielefeld University, North Rhine-Westphalia, Germany. Correspondence to: Feng Zheng <zhengf@sustech.edu.cn>, Yaochu Jin <yaochu.jin@surrey.ac.uk>.

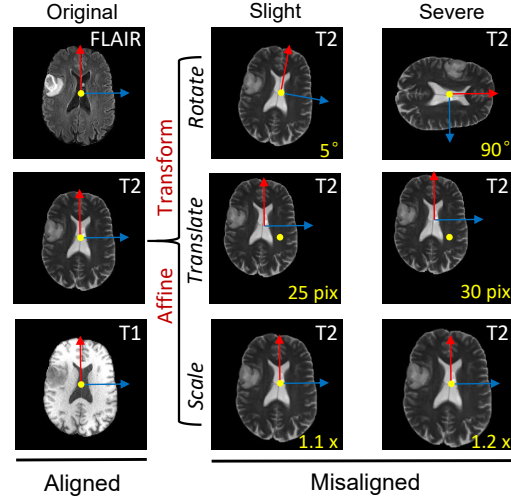


Figure 1. Illustration of multi-modal images, including slightly and severely misaligned cases, paired and unpaired cases.

1. Introduction

The majority of existing medical datasets (ixi; Siegel et al., 2019; Bakas et al., 2017), especially for neuroimaging data, are high-dimensional and heterogeneous. For instance, positron emission tomography (PET) and magnetic resonance imaging (MRI) are the imaging techniques to measure the information of organs for auxiliary diagnosis or monitor treatment. The paired/registered multi-modal data provide more complementary information to investigate certain pathologies or neurodegenerations. However, it is not feasible to acquire a full set of completely paired and aligned multi-modal neuroimaging data since: 1) collecting multi-modal neuroimaging data is very costly, for example, a normal MRI can take more than one thousand dollars in New York; 2) many medical institutions cannot share their data, since medical data are especially restricted to the local regulations, despite the identifiable information having been removed for protecting the privacy of patients. 3) patients' motions may result in severe misaligned neuroimaging data. 4) state-of-the-art deformable registration algorithms require tens of minutes to hours for a pair of scans. Hence, most of the neuroimaging data dispersed into different hospitals are misaligned unpaired imaging data

(MUD). We deeply investigate the misaligned neuroimaging data in a realistic scenario. We can divide the misaligned phenomenon into three parts, severe rotation, severe translation, and severe rescaling, which can be referred from the second row of Fig. 1. The misaligned data setting is similar to RegGAN (Kong et al., 2021). But the difference is that the misaligned data setting of FedMed-ATL is more severe than the one in RegGAN. Specifically, the angle rotation setting, the translation setting and the rescaling setting in RegGAN are restricted in $[-5, +5]$ degrees, $[-25, +25]$ pixels and $[0.9, 1.1]$ ratios, respectively. But the angle rotation setting, the translation setting, and the rescaling setting range in $[-90, +90]$ degrees, $[-30, +30]$ pixels, and $[0.9, 1.2]$ ratios, respectively. In this paper, we simulate all possible MUD distribution settings and the detail can be referred to Section 4.

For decades, deformable registration is a fundamental task in medical misaligned imaging studies. Deformable registration aims to establish a dense and non-linear correspondence between a pair of images, such as 3D misaligned multi-modal neuroimaging data. Traditional methods (Avants et al., 2011; Klein et al., 2009) align each voxel with a similar appearance by enforcing constraints on the registration mapping. Most of the traditional deformable registration methods can obtain high accuracy. However, they require to spend very huge computation resources and are slow in practice. Guha et al. (Balakrishnan et al., 2019) adopts a CNN method to speed up the whole registration procedure. In specific, the work in (Balakrishnan et al., 2019) parameterizes the original deformable registration method as a CNN and optimizes the parameters of CNN via a set of paired but misaligned images. But the doctors need to verify the effect of deformation algorithms by themselves. So it inevitably results in a huge amount of labor work and long checking time. Therefore, the emerging issue is how to utilize MUD but without deformable registration to facilitate brain inter-modality image synthesis. Closest to FedMed-ATL, RegGAN (Kong et al., 2021) forms the misaligned images as the noisy label and utilizes the correction loss to minimize the error resulting from misalignment. However, the assumption of RegGAN (Kong et al., 2021) is that the neuroimaging data meets with slight distortion. In this case, RegGAN can convert the slight-distorted neuroimaging data as the noisy label. But in reality, some of the misaligned neuroimaging data inevitably meets with severe distortion. Thus, FedMed-ATL eliminates the requirements of RegGAN and seems MUD as multi-view data augmentation for discriminator training, which can significantly mitigate the mode collapse due to the side effect from MUD. Inspired by (Chen et al., 2020d), FedMed-ATL reuse the discriminator as the encoder. More augmented views of MUD are generated by Affine Transform Module and fed into our designed auxiliary heads, including auxiliary rotation head,

auxiliary translation head and auxiliary rotation head. This action aims to enhance the discriminator’s ability to distinguish the real and fake samples. We heuristically prove that FedMed-ATL outperforms RegGAN significantly in a severe distortion setting. Figure 2 goes in detail.

Another issue for multi-modality brain image synthesis is data isolation and privacy concern. Even in multi-hospital collaborative research, they would undertake integrated analysis rather than sharing research data with other hospitals. Lately, a large amount of effort has been made to facilitate the availability of medical data without violating the privacy issue. Federated Learning (FL) is one of the popular approaches. FL is a decentralized approach where local clients train their local models without transmitting data to a central server, and the global model aggregates the gradients from clients (McMahan et al., 2017b). In addition, FL with GANs has witnessed some pilot progress on image synthesis (Chen et al., 2020b; Augenstein et al., 2019; Song & Ye, 2021). For example, DP-FedAvg-GAN (Augenstein et al., 2019) trains GANs with the differential privacy-preserving algorithm, which clips the gradients to bound sensitivity and adds calibrated random noise to introduce stochasticity. Closest to our work is FedMed-GAN (Xie et al., 2022). But they assume that all of the neuroimaging data are very clean, i.e., well-aligned in their experimental settings. While FedMed-ATL assumes all neuroimaging data from each hospital are MUD. We find that FedMed-ATL surpasses FedMed-GAN when each clients’ data are MUD. In addition, we also make a more comprehensive consideration in a realistic scenario and gives more assumption for all possible data distribution settings and data misaligned conditions. For example, we assume that some hospitals’ data are misaligned but paired data and the others are well aligned and paired data. In other words, we need to consider supervised and unsupervised GAN integrated into federated learning. In this case, we also find that the performance of FedMed-ATL is better than FedMed-GAN.

Our contributions can be summarized as follows:

- To the best of our knowledge, FedMed-ATL is the first algorithm to make use of the severely misaligned unpaired data (MUD) to facilitate the multi-modality brain synthesis. FedMed-ATL reduces the demand for the deformable registration when neuroimaging data meet severe distortions.
- Inspired by self-supervised learning, FedMed-ATL treats MUD as a multi-view data augmentation procedure rather than noisy data. We propose four auxiliary losses to the discriminator, including auxiliary rotation, auxiliary translation, auxiliary rescaling losses (termed as the Affine Transform Loss). The propose method shows good quality of synthesized results under a severely misaligned and unpaired data setting,

and better stability than other Medical-GAN-based algorithms.

- FedMed-ATL encourages to realize the usage of those misaligned and unpaired data when compared with RegGAN, like 90° rotation and 20% translation. Besides, FedMed-ATL exceeds FedMed-RegGAN by a big margin when severe distortions occurs in both misaligned and unpaired neuroimaging data.

2. Related Work

Medical Image-to-Image Translation Image-to-image translation (I2IT) aims to take images from one domain and translate them into images with a style (or characteristics) of another domain. It is first proposed in (Isola et al., 2017). In specific, the Pix2Pix mode (Isola et al., 2017) demands the use of well-aligned paired images, which are not always available. CycleGAN (Zhu et al., 2017) extends the generative framework to unpaired data and is capable of accomplishing unsupervised I2IT. Based on the cycle-consistency mode, many variants have been proposed. UNIT (Liu et al., 2017) makes use of two VAE encoders to map images from disparate domains into a common space. MUNIT (Huang et al., 2018a) and DRIT (Lee et al., 2018; 2020) disentangle content and style code to promote a variety of styles. Similarly, FUNIT (Liu et al., 2019) extends prior work in the area of few-shot scenarios and the model can be applied to a variety of domains with only a few examples in each. NICEGAN (Chen et al., 2020c) suggests that the discriminator can be reused for encoding.

The existing medical image to image translation (Zhang et al., 2018; Yu et al., 2019; Zhang et al., 2018; Jiang et al., 2019; Ren et al., 2021) has demonstrated considerable prospects for both research and clinical analysis. Huang et al. (Huang et al., 2021) proposed an unsupervised multi-variate canonical $CSC\ell_4$ Net to perform cross-modal image synthesis considering both intra-modal and inter-modal heterogeneity. Kong et al. (Kong et al., 2021) introduced a new I2IT model called RegGAN, which converts the unsupervised I2IT task into a supervised I2IT with noisy labels. But RegGAN does not deal with the severe distortion, which may happen in the realistic scenario.

Medical Image Deformable Registration There is a lot of work for medical image registration, including statistical parametric mapping (Ashburner & Friston, 2000), elastic deformation model (Bajcsy & Kovačič, 1989; Shen & Davatzikos, 2002), B-spline (Rueckert et al., 1999), Demons (Thirion, 1998; Pennec et al., 1999) and discrete methods (Dalca et al., 2016). Closest to our work is Arar et al. (Arar et al., 2020) and Kong et al. (Kong et al., 2021). The work in (Arar et al., 2020) apply an image-to-image translation network to preserve the geometric prop-

erty, which may be lost from deformable regularization. But their work aims to obtain better registration results but not for the image synthesis.

Federated Learning Federated learning, as a privacy-preserving decentralized learning strategy, allows clients to train their models without communicating data to a central server, and the global model is updated by aggregating client updates. FedAvg (McMahan et al., 2017a) combines local stochastic gradient descent (SGD) on each client with a server that performs model averaging. Yurochkin et al. (Yurochkin et al., 2019) developed a Bayesian non-parametric framework for federated learning with neural networks. FedProx (Li et al., 2020) provides a generalized and re-parametrized FedAvg that addresses the challenges of heterogeneity both theoretically and empirically. FedMA (Wang et al., 2020) constructs the shared global model in a layer-wise manner by matching and averaging hidden elements with similar feature extraction signatures.

Incorporating the generative adversarial framework into federated learning is challenging, since the cost functions may not converge using federated gradient aggregation in a minimax game between the discriminator and the generator. Several studies (Augenstein et al., 2020; Chen et al., 2020a; Song & Ye, 2021) have attempted to integrate the GAN-based framework with the federated learning. DP-FedAvg-GAN (Augenstein et al., 2020) trains GANs for image synthesis with differential privacy guarantees. In DP-FedAvg-GAN, the server holds a shared generator and discriminator that are delivered to clients. GS-WGAN (Chen et al., 2020a) enables the release of a sanitized version of sensitive data while maintaining stringent privacy protections. GS-WGAN is capable of more precisely distorting gradient information, allowing for the training of deeper models that generate more informative samples. FedMed-ATL shares a similar federated setting with FedMed-GAN (Xie et al., 2022). But Xie et al. (Xie et al., 2022) employs an edge loss to increase the quality of synthesis brain image, which may have a side effect for clinical diagnosis since edges mismatches and differences between modalities may be used as key diagnostic criteria.

3. Our FedMed-ATL

This section presents a detailed formulation of FedMed-ATL, which can be referred to Figure 2.

3.1. Federated Model Setup

The federated setting of FedMed-ATL’s generator and discriminator is described in Figure 3. We employ CycleGAN (Zhu et al., 2017), MUNIT (Huang et al., 2018b) and UNIT (Liu et al., 2017) as our baseline models. The task of FedMed-ATL is to generate a B-modal image by inputting

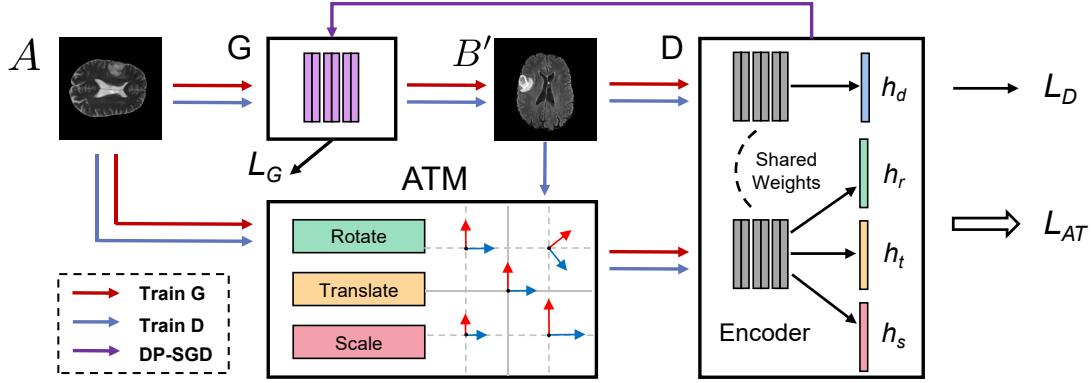


Figure 2. The pipeline of FedMed-ATL. The generator G generates B-modal images B' from A-modal. The discriminator D distinguishes B' from real or fake. The affine transform module (ATM) achieves image transform. The functions of L_G , L_D , and L_{AT} are the generator loss, the discriminator loss, and the affine transform loss, respectively. To train G and D , the red line and blue line describe the data flow. Note that input A-model images are fed into G and ATM for training G , but both input A-model images and generated B-model images B' are fed into D . In ATM, three transform blocks (Rotate, Translate, Scale) provide a rich data resource. For federated learning, we add DP-SGD (Abadi et al., 2016) (purple line) to avoid privacy leakage.

an A-modal image.

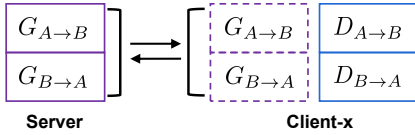


Figure 3. The federated setting of FedMed-ATL model. G denotes the shared generator and D denotes the discriminator.

CycleGAN (Zhu et al., 2017) owns two generators and discriminators. $G_{A \rightarrow B}$ denotes that the role of the generator is to generate B-modal images from A-modal samples. While $G_{B \rightarrow A}$ means that the role of the generator is to generate A-modal data from B-modal images. $D_{A \rightarrow B}$ denotes that the role of the discriminator is to distinguish whether B-modal data generated from A-modal samples is fake. $D_{B \rightarrow A}$ denotes that the role of the discriminator is to distinguish whether A-modal data generated from B-modal images is fake. The federated setting of CycleGAN is to locate two generators ($G_{A \rightarrow B}$ and $G_{B \rightarrow A}$) into the servers. It means that these two generators and edge-net of each hospital are aggregated into the server’s generators and edge-net. The server will also send its generators and edge-net into different hospitals after aggregation. The discriminators ($D_{A \rightarrow B}$ and $D_{B \rightarrow A}$) of each hospital are not shared with others.

In MUNIT (Huang et al., 2018b), there are two encoders (Enc_A and Enc_B), two decoders (Dec_A and Dec_B) and two discriminators ($D_{A \rightarrow B}$ and $D_{B \rightarrow A}$). The federated setting of MUNIT is to locate two encoders (Enc_A and Enc_B) and decoders (Dec_A and Dec_B) into the server. However, the discriminators of each hospital are not shared. In UNIT (Liu et al., 2017), there are two encoders ($E_{A \rightarrow B}$

and $E_{B \rightarrow A}$), two generators ($G_{A \rightarrow B}$ and $G_{B \rightarrow A}$) and two discriminators ($D_{A \rightarrow B}$ and $D_{B \rightarrow A}$). The federated setting of UNIT is to locate the encoders ($E_{A \rightarrow B}$ and $E_{B \rightarrow A}$), generators ($G_{A \rightarrow B}$ and $G_{B \rightarrow A}$) to the server. The federated settings of discriminators ($D_{A \rightarrow B}$ and $D_{B \rightarrow A}$) are the same as the ones in MUNIT. Note that we illustrate how to train for each client, due to the page limitation, so we put the server’s aggregation and resend algorithm into the Supplementary Material.

3.2. Misaligned Unpaired Data (MUD) Distribution

In real life, we address our task of federated self-supervised learning for MUD by formulating realistic settings. To simulate the real data distribution as much as possible, we adopt the following settings as shown in Figure 4.

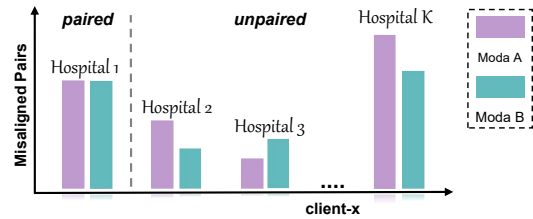


Figure 4. Distribution of misaligned unpaired data (MUD). For instance, Hospital 1 has paired data with misaligned attributes, while Hospitals of 2-K have MUD in the most real-life case.

Firstly, we divide ready-made data into several clients, where each client has its own private and unique data. At the same time, these clients (hospitals) contain unbalanced multi-modal images, i.e. have different numbers of patients in each client or have different numbers of images in each

modality. Secondly, without losing generality, there are paired and unpaired cases in our settings. For example, we randomly select the multi-modal slices from the same patient as paired data like in Hospital 1 or select them from patients with different IDs as unpaired data like in Hospital 2. Lastly, we randomly transform input images at a certain threshold of rotation, translation, and scaling, and there is the majority of misaligned images in the constructed training set.

3.3. Network Architectures

Generator In Figure 2, the architecture of generator is the same as CycleGAN (Zhu et al., 2017), MUNIT (Huang et al., 2018a) and UNIT (Liu et al., 2017). Specifically, the encoder and decoders of MUNIT and UNIT are regarded as the generators in Figure 2.

Discriminator Inspired by Chen *et al.* (Chen et al., 2020d), FedMed-ATL reuses the original discriminator as the encoder. The architecture of discriminator that except for the last layer is the same as CycleGAN (Zhu et al., 2017), MUNIT (Huang et al., 2018a) and UNIT (Liu et al., 2017). FedMed-ATL replaces the last layer of origin discriminator with a two-layer MLP (termed as discriminator head). In Figure 2, h_d represents the discriminator head. The input and output dimension of two layers are (512-128), (128, 1). The role of the discriminator head is to distinguish the real or fake samples.

Affine Transform Module (ATM) ATM contains three operators, namely rotation, translation, and rescaling. As for rotations, the rotation degree is chosen in $[0^\circ, 90^\circ, 180^\circ, 270^\circ]$. As for translation, the x-axis and y-axis translation is chosen in $[(-30, -30), (-30, 30), (30, -30), (30, 30)]$. As for rescaling, the scaling ratio is chosen in $[0.9, 1.1, 1.2]$. We conduct a comprehensive ablation study on the number of views for each operation. The number of views is a range in $[1, 2, 4]$. For instance, if the number of views is 4, FedMed-ATL picks 4 augmented views from rotation, translation, and rescaling and feeds them into auxiliary rotation head, auxiliary translation head, and auxiliary rescaling head. In addition, when FedMed-ATL trains the generators, only the real samples are fed into ATM. While the real and fake samples are fed into the ATM when FedMed-ATL trains the discriminator. The action is to prevent the generated samples to be easily detected by the discriminator. In other words, FedMed-ATL encourages the generator to generate more 'real misaligned' detectable samples for the discriminator to avoid the discriminator being overfitting.

Auxiliary Rotation Head The role of auxiliary rotation head (h_r in Figure 2) is to distinguish the rotation angle of the neuroimaging data, i.e., $0^\circ, 90^\circ, 180^\circ$ and 270° . Before going into the auxiliary rotation head, FedMed-ATL needs to feed them into the encoder. This encoder is shared with

the other heads, including the discriminator head, translation head, and scaling head. In Equation 1, x are the real samples when FedMed-ATL update the parameters of generators. While x in Equation 1 are both the real sample and fake samples (the generated samples) when FedMed-ATL updates the parameters of discriminators. $P_{h_r}(R|x^r)$ is the auxiliary rotation head's predictive distribution over the angles of rotation of the sample. The intuition of auxiliary rotation loss is to let the discriminator see more severe rotated samples. Since the rotation head and discriminator head share the same encoder, i.e., these two heads own similar features. In this case, even if the discriminator meets with the severely rotated samples, auxiliary rotation loss could help the discriminator to distinguish real or fake samples without being affected by severe rotation.

Auxiliary Translation Head The role of auxiliary translation head (h_t in Figure 2) is to distinguish the translation distance of the neuroimaging data, i.e., $[(-30, -30), (-30, 30), (30, -30), (30, 30)]$. x are the real samples when FedMed-ATL updates the parameters of generators. While x in Equation 2 are both the real sample and fake samples (the generated samples) when FedMed-ATL updates the parameters of discriminators. $P_{h_t}(T|x^t)$ is the auxiliary translation head's predictive distribution over the translation direction and distance of the sample. The aim of auxiliary translation loss is similar to the auxiliary rotation loss. In this case, the discriminator meets with the severe translated samples, auxiliary translation loss could help the discriminator to distinguish real or fake samples without being affected by severe translation.

Auxiliary Rescaling Head The role of auxiliary rescaling head (h_s in Figure 2) is to distinguish the rescaling ratio of the neuroimaging data, i.e., $[0.9, 1.1, 1.2]$. x are the real samples when FedMed-ATL updates the parameters of generators. While x in Equation 3 are both the real sample and fake samples (the generated samples) when FedMed-ATL updates the parameters of discriminators. $P_{h_s}(S|x^s)$ is the auxiliary rescaling head's predictive distribution over the scaling ratio of the sample. The aim of auxiliary rescaling loss is similar to the auxiliary rotation loss. Auxiliary scaling loss could help the discriminator to distinguish real or fake samples without being affected by severe rescaling.

3.4. Loss Function

AT Loss Three affine transform modes, namely rotation, translation, and scaling, are defined as follows.

$$L_{rot} = \lambda_{rot} \cdot \mathbb{E}[\log P_{h_r}(R = r|x^r)] \quad (1)$$

$$L_{trans} = \lambda_{trans} \cdot \mathbb{E}[\log P_{h_t}(T = t|x^t)] \quad (2)$$

$$L_{scale} = \lambda_{scale} \cdot \mathbb{E}[\log P_{h_s}(S = s|x^s)] \quad (3)$$

GAN and Cycle Loss Equation (4) is GAN loss function (Isola et al., 2017), where G is the generator that generate B-modal images from A-modal images and D is the discriminator that distinguish whether B-modal images generated from A-modal samples is fake.

$$\min_G \max_G L_{adv}(G, D) = \mathbb{E}_y[\log(D(y))] + \mathbb{E}_x[\log(1 - D(G(x)))] \quad (4)$$

Equation (5) is Cycle loss function (Zhu et al., 2017), where F is the generator that generate A-modal image from B-modal images.

$$\min_G \max_G L_{cyc}(G, F) = \mathbb{E}_x[||F(G(x)) - x||_1] + \mathbb{E}_y[||G(F(y)) - y||_1] \quad (5)$$

Total Loss Overall, the total loss function is defined as:

$$L_{total} = \lambda_{rot} \cdot L_{rot} + \lambda_{trans} \cdot L_{trans} + \lambda_{scale} \cdot L_{scale} + \lambda_{adv} \cdot L_{adv} + \lambda_{cyc} \cdot L_{cyc}. \quad (6)$$

The weight λ of various loss functions will be introduced in Section 4. Note that due to the page limitation, we put the whole training algorithm into Supplementary Material.

4. Experiments

4.1. Federated Settings

IXI (ixi) collects nearly 600 MR images from normal and healthy subjects at three hospitals. The MR image acquisition protocol for each subject includes T1, T2, PD-weighted images (PD), MRA images, and Diffusion-weighted images (15 directions). Here, we only use T1 (581 cases), T2 (578 cases), and PD (578 cases) data to conduct our experiments, and select the paired data with the same ID from the three modes. The image has a non-uniform length on the z-axis with the size of 256 on the x-axis and y-axis. The IXI data set is not divided into a training set and a test set. Therefore, we randomly split the whole data as the training set (0.8) and the test set (0.2).

BraTS2021 (Siegel et al., 2019; Bakas et al., 2017) is constructed for analysis and diagnosis of brain disease. The publicly available dataset of multi-institutional pre-operative MRI sequences is provided: training (1251 cases) and validation (219 cases). Each patient contributes $155 \times 240 \times 240$ with four sequences: T1, T2, T1ce, and FLAIR.

Data processing To ensure data validity and diversity by removing a skull without tissues in a slice, we split the three-dimensional volume and select slices from 50 to 80 on the Z-axis. All of the images of the two datasets are cropped into the size of 256 pixels. Here, we define unpaired data

as two modal slices (T1, FLAIR) from two volumes (A and B) but with the same N-th slice, e.g., unpaired data [T1-A-N, FLAIR-B-N]. By affinely transforming $at(\cdot)$ both two modal images, we obtain a MUD like $[at(T1-A-N), at(FLAIR-B-N)]$. In our federated scenario, we first divide the training data (volume) proportionally into 4 clients based on the size of client data [0.4, 0.3, 0.2, 0.1], where each client has its own private and unique ones. After that, we construct MUDs in each client via the generation principle of unpaired data and misaligned data. In training, we select overall 6,000 images as the IXI and BraTS2021 training data, and each client selects 2,400, 1,800, 1,200, and 600 from its database, respectively. For evaluation, we use 3,462 images as the IXI validation data, and 6,570 images as the BraTS2021 validation data.

Metrics We employ three metrics to evaluate our generator’s performance, mean absolute error (MAE), peak signal ratio (PSNR), and structural similarity index (SSIM). The lower MAE, the higher PSNR and SSIM denotes the higher quality of the synthesis image. The details of these three metrics are described in Supplementary Material.

Implementations In the federated scenario, there are 4 clients in our experiment, and the number of volumes owned by each client is 0.4 0.3, 0.2, and 0.1 respectively. We run 3 rounds for federated training, and each client is trained for 3 epochs. The model aggregation strategy is Fed-Avg (McMahan et al., 2017b), which aggregates the weight from each client’s generator model to the server model according to the data proportion distribution for each client. Specifically, we use the learning rate of $1e - 4$ and the batch size of 4. The optimizer is Adam (Kingma & Ba, 2014). Its beta1 and beta2 are 0.5 and 0.999, respectively. The weights of GAN loss λ_{adv} and Cycle loss λ_{cyc} are 1.0, 10.0, respectively. For the affine transform loss (ATL), we set weights of rotation λ_{rot} , translation λ_{trans} , and scaling λ_{scale} to 1.0 for each model’s generator and 0.5 for its discriminator, respectively. In FedMed-ATL differential privacy settings, the level of gradient clip bound, sensitivity, and noise multiplier is fixed to 1.0, 2.0, and 1.07, respectively. In terms of differential privacy setting, the Gaussian noise μ is set to 1.07, and the standard deviation σ is set to 2.0. The clip bound for the back-propagation gradient is set to 1.0.

Slight and Severe Noise Slight noise denotes the noise level is 3 in RegGAN (Kong et al., 2021) setting. In specific, slight noise denotes the angle ranges in $[-3^\circ, 3^\circ]$, the translation ranges in $[-15, +15]$ pixels and the scaling ratio ranges in $[0.9, 1.1]$. Severe noise denotes that the angle ranges in $[-90^\circ, 90^\circ]$, the translation ranges in $[-30, +30]$ pixels and the scaling ratio ranges in $[0.9, 1.2]$, respectively.

Table 1. Comparison results of modal generation (from PD to T2) on the IXI dataset.

Method	Slight Noise			Severe Noise		
	MAE ↓	PSNR ↑	SSIM ↑	MAE ↓	PSNR ↑	SSIM ↑
FedMed-C (+reggan)	0.0294	26.0068	0.9614	0.0302	24.5915	0.9477
FedMed-C	0.0385	24.9238	0.9545	0.0295	25.0715	0.9555
FedMed-C-ATL	0.0279	25.0844	0.9560	0.0290	24.7132	0.9517

Table 2. Comparison results of modal generation (from T1 to FLAIR) on the BraTS2021 dataset.

Method	Slight Noise			Severe Noise		
	MAE ↓	PSNR ↑	SSIM ↑	MAE ↓	PSNR ↑	SSIM ↑
FedMed-C (+reggan)	0.0481	19.8538	0.8841	0.0455	20.0179	0.8950
FedMed-C	0.0466	20.0601	0.9003	0.0474	19.9319	0.8928
FedMed-C-ATL	0.0447	20.3961	0.9044	0.0439	20.8232	0.9123

4.2. Main Results

We introduce the notation used in Table 1, Table 2, Table 3, and Table 4. To begin with, M, C and U are the short names for MUNIT (Huang et al., 2018a), CycleGAN (Zhu et al., 2017) and UNIT (Liu et al., 2017), respectively.

FedMed-C denotes that we only put CycleGAN into our federated settings, which introduced in Section 3.1 and Section 4.1. FedMed-C only adopts cycle loss (5) and adversarial loss (4). **FedMed-C (+reggan)** denotes that FedMed-C adopts the correction loss and registration network that introduced in RegGAN (Kong et al., 2021). **FedMed-C-ATL** denotes that FedMed-C employs the affine transform loss (ATL), which is introduced in Equation (6).

Table 1 and Table 3 show the results of generating T2 from PD in IXI dataset. Table 2 and Table 4 show the results of generating FLAIR from T1 in BraTS2021 dataset. And the loss Note that due to the page limitation, we put the experiments of MUNIT and UNIT and the other modalities in IXI and BraTS2021 into the Supplementary Material.

4.3. Ablation Study

Analysis of ATL To evaluate the affine transform loss, we test rotation, translation, and scaling, respectively. **FedMed-C-AR** denotes that FedMed-C just employs the auxiliary rotation loss, which is introduced in Equation (1). **FedMed-C-AT** denotes that FedMed-C just employs the auxiliary translation loss, which is introduced in Equation (2). **FedMed-C-AS** denotes that FedMed-C just employs the auxiliary scaling loss, which is introduced in Equation (3).

Analysis of Different Views in ATL We further investigate the impact of different views on ATL. **FedMed-C-ATL-1View** denotes that FedMed-C-ATL randomly picks one augmented view from ATM Module and feeds it into the encoder (discriminator), which is described in Figure 2 and Section 3.3. In other words, there is only one augmented view to feed into auxiliary rotation head, auxiliary translation head, and auxiliary rescaling head, respectively.

FedMed-C-ATL-2Views denotes that FedMed-C-ATL randomly picks two augmented views and feeds them into the encoder (discriminator). The specific operation is similar to FedMed-C-ATL-1View, but the number of views is 2. **FedMed-C-ATL-4Views** denotes that FedMed-C-ATL picks four augmented views and feeds them into the encoder (discriminator). Note that in the previous description, the default way is to pick 4 views if this paper does not mention the number of views explicitly.

Key Findings 1 We compare FedMed-C-ATL with a previous state-of-the-art algorithm, i.e. RegGAN (Kong et al., 2021). It can be observed that FedMed-C-ATL outperforms FedMed-RegGAN by a large margin in a severe MUD setting, which achieves 2.4 % - 4.6 % absolute improvements in MAE, PSNR, and SSIM, respectively. The results demonstrate that FedMed-C-ATL has a better ability to facilitate the quality of the synthesis, even if the input data suffered from a severe distortion. In addition, FedMed-C-ATL achieves absolute improvements of 10 %, 2.7 % and 2.7 % in slight MUD settings when compared with FedMed+RegGAN. The improvement demonstrates the effectiveness of our FedMed-C-ATL for the slight MUD scenario. We also observe that FedMed-C performs slightly better than FedMed-C-ATL in the severe MUD settings on the IXI dataset. The principal reason is that data augmentation of FedMed-C-ATL may result in the opposite effect when facing a very clean dataset like IXI. Here, “clean” does not mean a well-aligned and paired dataset. It means the data collected from healthy persons. Too many data augmentation treatments for a clean dataset are meaningless and even harmful for the synthesis algorithm.

Key Findings 2 To further evaluate the effectiveness of FedMed-C-ATL, we make a further ablation study to verify the usefulness of various auxiliary heads. From Table 4, It can be observed that adding more heads could improve better performance in a severe MUD setting. In specific, FedMed-C-ATL-4views outperforms FedMed-C-AS by a large margin in a severe MUD setting, which achieves 6.8 %,

Table 3. Results of modal generation (from PD to T2) on the IXI dataset.

Method	Slight Noise			Severe Noise		
	MAE ↓	PSNR ↑	SSIM ↑	MAE ↓	PSNR ↑	SSIM ↑
FedMed-C	0.0385	24.9238	0.9545	0.0295	25.0715	0.9555
FedMed-C-AR	0.0261	25.3358	0.9577	0.0298	24.3385	0.9467
FedMed-C-AT	0.0271	25.2926	0.9569	0.0291	24.7600	0.9509
FedMed-C-AS	0.0297	24.7426	0.9508	0.0316	24.0586	0.9410
FedMed-C-ATL-1View	0.0311	24.7486	0.9562	0.0331	24.2766	0.9518
FedMed-C-ATL-2Views	0.0288	24.8814	0.9562	0.0305	24.3427	0.9488
FedMed-C-ATL-4Views	0.0279	25.0844	0.9560	0.0290	24.7132	0.9517

Table 4. Results of modal generation (from T1 to FLAIR) on the BraTS2021 dataset.

Method	Slight Noise			Severe Noise		
	MAE ↓	PSNR ↑	SSIM ↑	MAE ↓	PSNR ↑	SSIM ↑
FedMed-C	0.0466	20.0601	0.9003	0.0474	19.9319	0.8928
FedMed-C-AR	0.0483	19.9217	0.8904	0.0439	20.4555	0.9056
FedMed-C-AT	0.0466	20.2059	0.8944	0.0440	20.4512	0.9042
FedMed-C-AS	0.0459	20.0981	0.8956	0.0435	20.6446	0.9093
FedMed-C-ATL-1View	0.0451	20.6151	0.9085	0.0439	20.8199	0.9115
FedMed-C-ATL-2Views	0.0451	20.2883	0.9012	0.0459	20.4236	0.9047
FedMed-C-ATL-4Views	0.0447	20.3961	0.9044	0.0439	20.8232	0.9123

1.7 % and 1.1 % absolute improvements in MAE, PSNR, and SSIM, respectively. From Table 3, FedMed-C-ATL-4views surpasses FedMed-C-AS by 1.1 % and 2.1 % in MAE, PSNR and SSIM, respectively.

Key Findings 3 Furthermore, we desire to understand how important it is for the number of data augmentation. From Table 4 and Table 3, it can be observed that FedMed-C-ATL-4views outperforms FedMed-C-ATL-1view and FedMed-C-ATL-2views in severe MUD settings. For example, FedMed-C-ATL-4views outperforms FedMed-C-ATL-1view by 1.2 %, 2.1 % and 2.7 % in MAE, PSNR, and SSIM, respectively. It demonstrates that the number of data augmentation plays a positive role in the quality of synthesis image, especially in severe MUD settings.

4.4. Visualization

To present the performance of synthesized images by our federated mode (FedMed), we draw the generated results of FedMed-C (+reggan) and FedMed-C-ATL in Figure 5. From the results, we can see that FedMed-C has the ability to generate high-quality images, where the texture information of tissues and modal style would be well maintained. Importantly, our FedMed can deal with severely misaligned unpaired input cases.

5. Conclusions

In realistic scenario, the misaligned and unpaired neuroimaging data (MUD) are inevitable. But the traditional deformable registration methods requires expensive computational power. From our perspectives, MUD can be regarded

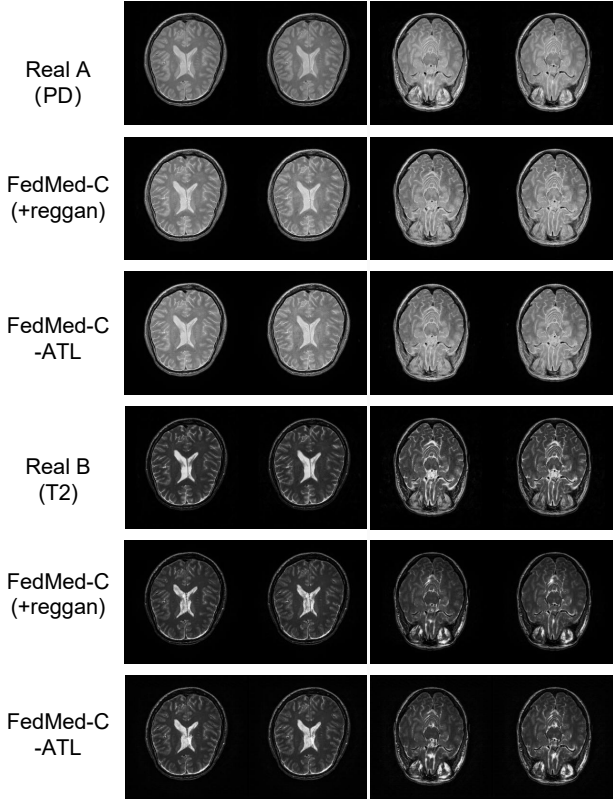


Figure 5. Visualization of brain images generated by FedMed-C (+reggan) and FedMed-C-ATL on the IXI Validation set. The model is trained on the severe noise scheme. The row images represent two volume examples of two near slices.

as data augmentation and can be an important manner to increase the quality of synthesis neuroimaging data. FedMed-ATL provides a simple but effective way to facilitate multi-modal brain image synthesis. We prove that FedMed-ATL outperforms state-of-the-art algorithm when data in severe MUD settings. Hopefully FedMed-ATL could motivate the medical GAN community to focus on severe MUD scenario.

References

- Ixi dataset. <https://brain-development.org/ixi-dataset/>.
- Abadi, M., Chu, A., Goodfellow, I., McMahan, H. B., Mironov, I., Talwar, K., and Zhang, L. Deep learning with differential privacy. In *Proceedings of the 2016 ACM SIGSAC conference on computer and communications security*, pp. 308–318, 2016.
- Arar, M., Ginger, Y., Danon, D., Bermano, A. H., and Cohen-Or, D. Unsupervised multi-modal image registration via geometry preserving image-to-image translation. In *Proceedings of the IEEE/CVF conference on computer vision and pattern recognition*, pp. 13410–13419, 2020.
- Ashburner, J. and Friston, K. J. Voxel-based morphometry—the methods. *Neuroimage*, 11(6):805–821, 2000.
- Augenstein, S., McMahan, H. B., Ramage, D., Ramaswamy, S., Kairouz, P., Chen, M., Mathews, R., et al. Generative models for effective ml on private, decentralized datasets. *arXiv preprint arXiv:1911.06679*, 2019.
- Augenstein, S., McMahan, H. B., Ramage, D., Ramaswamy, S., Kairouz, P., Chen, M., Mathews, R., and y Arcas, B. A. Generative models for effective ML on private, decentralized datasets. In *ICLR*. OpenReview.net, 2020.
- Avants, B. B., Tustison, N. J., Song, G., Cook, P. A., Klein, A., and Gee, J. C. A reproducible evaluation of ants similarity metric performance in brain image registration. *Neuroimage*, 54(3):2033–2044, 2011.
- Bajcsy, R. and Kovačič, S. Multiresolution elastic matching. *Computer vision, graphics, and image processing*, 46(1): 1–21, 1989.
- Bakas, S., Kuijff, H. J., Menze, B. H., and Reyes, M. Brain-lesion: Glioma, multiple sclerosis, stroke and traumatic brain injuries. In *Lecture Notes in Computer Science*, 2017.
- Balakrishnan, G., Zhao, A., Sabuncu, M. R., Guttag, J., and Dalca, A. V. Voxelmorph: a learning framework for deformable medical image registration. *IEEE transactions on medical imaging*, 38(8):1788–1800, 2019.
- Chen, D., Orekondy, T., and Fritz, M. GS-WGAN: A gradient-sanitized approach for learning differentially private generators. In *NeurIPS*, 2020a.
- Chen, D., Orekondy, T., and Fritz, M. Gs-wgan: A gradient-sanitized approach for learning differentially private generators. *arXiv preprint arXiv:2006.08265*, 2020b.
- Chen, R., Huang, W., Huang, B., Sun, F., and Fang, B. Reusing discriminators for encoding: Towards unsupervised image-to-image translation. In *CVPR*, pp. 8165–8174. Computer Vision Foundation / IEEE, 2020c.
- Chen, R., Huang, W., Huang, B., Sun, F., and Fang, B. Reusing discriminators for encoding: Towards unsupervised image-to-image translation. In *Proceedings of the IEEE/CVF Conference on Computer Vision and Pattern Recognition*, pp. 8168–8177, 2020d.
- Dalca, A. V., Bobu, A., Rost, N. S., and Golland, P. Patch-based discrete registration of clinical brain images. In *International Workshop on Patch-based Techniques in Medical Imaging*, pp. 60–67. Springer, 2016.
- Huang, X., Liu, M., Belongie, S. J., and Kautz, J. Multimodal unsupervised image-to-image translation. In *ECCV (3)*, volume 11207 of *Lecture Notes in Computer Science*, pp. 179–196. Springer, 2018a.
- Huang, X., Liu, M.-Y., Belongie, S., and Kautz, J. Multimodal unsupervised image-to-image translation. In *Proceedings of the European conference on computer vision (ECCV)*, pp. 172–189, 2018b.
- Huang, Y., Zheng, F., Wang, D., Huang, W., Scott, M. R., and Shao, L. Brain image synthesis with unsupervised multivariate canonical csc4net. In *CVPR*, pp. 5881–5890. Computer Vision Foundation / IEEE, 2021.
- Isola, P., Zhu, J., Zhou, T., and Efros, A. A. Image-to-image translation with conditional adversarial networks. In *CVPR*, pp. 5967–5976. IEEE Computer Society, 2017.
- Jiang, G., Lu, Y., Wei, J., and Xu, Y. Synthesize mammogram from digital breast tomosynthesis with gradient guided cgans. In *International Conference on Medical Image Computing and Computer-Assisted Intervention*, pp. 801–809. Springer, 2019.
- Kingma, D. P. and Ba, J. Adam: A method for stochastic optimization. *arXiv preprint arXiv:1412.6980*, 2014.
- Klein, A., Andersson, J., Ardekani, B. A., Ashburner, J., Avants, B., Chiang, M.-C., Christensen, G. E., Collins, D. L., Gee, J., Hellier, P., et al. Evaluation of 14 nonlinear deformation algorithms applied to human brain mri registration. *Neuroimage*, 46(3):786–802, 2009.

- Kong, L., Lian, C., Huang, D., Li, Z., Hu, Y., and Zhou, Q. Breaking the dilemma of medical image-to-image translation, 2021.
- Lee, H., Tseng, H., Huang, J., Singh, M., and Yang, M. Diverse image-to-image translation via disentangled representations. In *ECCV (1)*, volume 11205 of *Lecture Notes in Computer Science*, pp. 36–52. Springer, 2018.
- Lee, H., Tseng, H., Mao, Q., Huang, J., Lu, Y., Singh, M., and Yang, M. DRIT++: diverse image-to-image translation via disentangled representations. *Int. J. Comput. Vis.*, 128(10):2402–2417, 2020.
- Li, T., Sahu, A. K., Zaheer, M., Sanjabi, M., Talwalkar, A., and Smith, V. Federated optimization in heterogeneous networks. In *MLSys*. mlsys.org, 2020.
- Liu, M., Breuel, T. M., and Kautz, J. Unsupervised image-to-image translation networks. In *NIPS*, pp. 700–708, 2017.
- Liu, M., Huang, X., Mallya, A., Karras, T., Aila, T., Lehtinen, J., and Kautz, J. Few-shot unsupervised image-to-image translation. In *ICCV*, pp. 10550–10559. IEEE, 2019.
- McMahan, B., Moore, E., Ramage, D., Hampson, S., and y Arcas, B. A. Communication-efficient learning of deep networks from decentralized data. In *AISTATS*, volume 54 of *Proceedings of Machine Learning Research*, pp. 1273–1282. PMLR, 2017a.
- McMahan, B., Moore, E., Ramage, D., Hampson, S., and y Arcas, B. A. Communication-efficient learning of deep networks from decentralized data. In *Artificial intelligence and statistics*, pp. 1273–1282. PMLR, 2017b.
- Pennec, X., Cachier, P., and Ayache, N. Understanding the “demon’s algorithm”: 3d non-rigid registration by gradient descent. In *International Conference on Medical Image Computing and Computer-Assisted Intervention*, pp. 597–605. Springer, 1999.
- Ren, M., Dey, N., Fishbaugh, J., and Gerig, G. Segmentation-renormalized deep feature modulation for unpaired image harmonization. *IEEE Transactions on Medical Imaging*, 40(6):1519–1530, 2021.
- Rueckert, D., Sonoda, L. I., Hayes, C., Hill, D. L., Leach, M. O., and Hawkes, D. J. Nonrigid registration using free-form deformations: application to breast mr images. *IEEE transactions on medical imaging*, 18(8):712–721, 1999.
- Shen, D. and Davatzikos, C. Hammer: hierarchical attribute matching mechanism for elastic registration. *IEEE transactions on medical imaging*, 21(11):1421–1439, 2002.
- Siegel, R. L., Miller, K. D., and Jemal, A. Cancer statistics, 2019. *CA: A Cancer Journal for Clinicians*, 69, 2019.
- Song, J. and Ye, J. C. Federated cyclegan for privacy-preserving image-to-image translation. *CoRR*, abs/2106.09246, 2021.
- Thirion, J.-P. Image matching as a diffusion process: an analogy with maxwell’s demons. *Medical image analysis*, 2(3):243–260, 1998.
- Wang, H., Yurochkin, M., Sun, Y., Papailiopoulos, D. S., and Khazaeni, Y. Federated learning with matched averaging. In *ICLR*. OpenReview.net, 2020.
- Xie, G., Wang, J., Huang, Y., Zheng, Y., Zheng, F., Song, J., and Jin, Y. Fedmed-gan: Federated multi-modal unsupervised brain image synthesis, 2022.
- Yu, B., Zhou, L., Wang, L., Shi, Y., Frapp, J., and Bourgeat, P. Ea-gans: edge-aware generative adversarial networks for cross-modality mr image synthesis. *IEEE transactions on medical imaging*, 38(7):1750–1762, 2019.
- Yurochkin, M., Agarwal, M., Ghosh, S., Greenewald, K. H., Hoang, T. N., and Khazaeni, Y. Bayesian nonparametric federated learning of neural networks. In *ICML*, volume 97 of *Proceedings of Machine Learning Research*, pp. 7252–7261. PMLR, 2019.
- Zhang, Z., Yang, L., and Zheng, Y. Translating and segmenting multimodal medical volumes with cycle-and shape-consistency generative adversarial network. In *Proceedings of the IEEE conference on computer vision and pattern Recognition*, pp. 9242–9251, 2018.
- Zhu, J.-Y., Park, T., Isola, P., and Efros, A. A. Unpaired image-to-image translation using cycle-consistent adversarial networks. In *Proceedings of the IEEE international conference on computer vision*, pp. 2223–2232, 2017.